Complex layered phases in asymmetric diblock copolymers

Ian Hamley, Mark Gehlsen, Ashish Khandpur, Kurt Koppi, Jeffrey Rosedale, Mark Schulz, Frank Bates, Kristoffer Almdal, Kell Mortensen

Classification
Physics Abstracts
61.12E — 61.30E — 61.40K — 64.80G

Complex layered phases in asymmetric diblock copolymers

Ian W. Hamley ([1,*]), Mark D. Gehlsen ([1]), Ashish K. Khandpur ([1]), Kurt A. Koppi ([1]), Jeffrey H. Rosedale ([1]), Mark F. Schulz ([1]), Frank S. Bates ([1,**]), Kristoffer Almdal ([2]) and Kell Mortensen ([2])

([1]) Department of Chemical Engineering and Materials Science, University of Minnesota, Minneapolis, MN 55455, U.S.A.
([2]) Risø National Laboratory, 4000 Roskilde, Denmark

(Received 21 June 1994, accepted 6 September 1994)

Abstract . — The phase behavior of diblock copolymers near the order-disorder transition is studied using transmission electron microscopy, small-angle neutron scattering (SANS) and dynamical mechanical spectroscopy. For a series of polyolefin diblocks with volume fraction, f_1, of the block with the larger segment length in the range $f_1 = 0.63 - 0.75$, we find that the transition from lamellae to hexagonally packed cylinder phases occurs *via* intermediate layered phases that are always characterized by in-plane hexagonal order. One class of diblock forms a hexagonally modulated lamellar (HML) phase, then a hexagonally perforated layer (HPL) phase upon heating from lamellae, while another class forms a modulated hexagonally packed cylinder phase from the HML phase. We attempt to rationalize this based on the differences in inter-layer ordering in the HML phase evidenced by SANS patterns. Detailed phase diagrams for the diblocks depend on molecular weight, and a conformational asymmetry parameter, which is discussed. These results are similar to those found in certain smectic liquid crystal polymorphs, suggesting an analogy between thermotropic liquid crystalline behavior and the intermediate layered phases of diblock copolymer melts.

1. Introduction.

The phase behavior of mesomorphic systems has been the subject of intense interest over the last quarter century. Thermotropic liquid crystal phases have been investigated in detail since the late 1960's and extensive experimental data and theoretical description is available for the structure and ordering of most of them. In contrast, the mesomorphism of lyotropic liquid crystals is less well understood. In particular, the driving forces for the formation of complex phases such as the bicontinuous cubic phases have not been elucidated in detail.

(*) Currently at Department of Physics, University of Durham, Science Laboratories, South Road, Durham, DH1 3LE, U.K.
(**) To whom correspondence should be addressed.

Schematically, in a binary amphiphile/solvent system these phases occur between the classical lamellar, hexagonally packed cylinder and spherical micelle phases [1].

Block copolymers are a class of mesomorphic systems of increasing interest due to their viscoelastic behavior and microphase segregation properties [2]. In the classical picture, a diblock copolymer can form lamellar, hexagonally packed cylinder, or body centered cubic phases, depending on the volume fraction of the two blocks. This is true for both strongly segregated and weakly segregated diblocks [3-5]. Experiments on strongly segregated block copolymers show phase behavior in quantitative agreement with the theory, except for the reported OBDD (Ordered Bicontinuous Double Diamond) morphology [6]. Hasegawa *et al.* have reported this structure for poly(styrene)-poly(isoprene) (PS-PI) diblocks with volume fractions $f_{PI} = 0.34$–0.38 in strongly segregated systems prepared by solvent casting [7].

In contrast to the classical phase behavior of strongly segregated block copolymers, it is becoming apparent that block copolymers near the order-disorder transition (ODT) show a much richer polymorphism [8]. Earlier work in this group focussed on a poly(ethylene-propylene)-poly(ethylethylene) (PEP-PEE) diblock copolymer with $f_{PEP} = 0.65$ [9]. Several ordered phases were identified on varying the temperature, using shear modulus measurements and small-angle neutron scattering (SANS) experiments [9]. Subsequently, the sequence of phase transitions on heating this system was identified as lamellae (LAM) - hexagonally modulated lamellae (HML) - hexagonally perforated layers (HPL) - hexagonally packed cylinders (HEX) [9]. The identification of these phases was facilitated by applying a reciprocating shear field to the block copolymers *in situ* at the SANS instrument. A specially constructed dynamic shearing device was used for this purpose [10].

Further work in this group has identified a different class of morpholgies for polyolefin diblock copolymers with $f_1 \cong 0.30$-0.45, where f_1 is the volume fraction of the block with the larger segment length (to be discussed), near the ODT. Small-angle neutron scattering, viscoelastic experiments, and transmission electron microscopy have indicated several new complex morphologies. We have observed a cubic structure localized near the ODT for $f_1 = 0.34$-0.43 in various diblock copolymers and diblock copolymer mixtures [8, 11-14]. In general, there appears to be two asymmetric regions of complex phase behavior in diblock copolymers, between lamellae and hexagonally packed cylinders on either side of the phase diagram. This is in striking analogy with the schematic phase diagram for binary surfactant/solvent systems given by Seddon [1]. Formally, diblock copolymer melts should be classified as thermotropic liquid crystals since they constitute single component systems that are influenced thermodynamically through variations in temperature (or pressure) at constant chemical composition.

Rather than attempt to summarize the full phase behavior of weakly segregated diblock copolymers, which is addressed elsewhere [8], we instead focus in this paper on the region of complex phase behavior between $f_1 = 0.60$ and $f_1 = 0.75$ in several polyolefin diblock copolymers. We have found that the transition from lamellae to hexagonally packed cylinders occurs *via* a variety of layered phases that are schematically shown in figure 1. Two classes of intermediate phases seem to exist at high f_1 in these systems, which are governed by the nature of the ordering in the intermediate hexagonally modulated lamellar (HML) phase. The controlling factor in determining two-dimensional or three-dimensional phase behavior appears to be the interlayer stacking behavior of the HML phase, which is illustrated in figure 2. The top view (x-z plane) in this figure shows two layers of an ABAB (hexagonal unit cell) stacking configuration. Side (x-y plane) and shear axis (y-z plane) views are identified with two independent parameters, d^*(interlayer spacing) and d'(in-plane modulation spacing). When this type of stacking produces well-defined three-dimensional hexagonal order, the system transforms into a hexagonal cylinder state upon heating. However, in many instances we find ill-defined stacking that can not be described in classical crystallographic terms, and then a

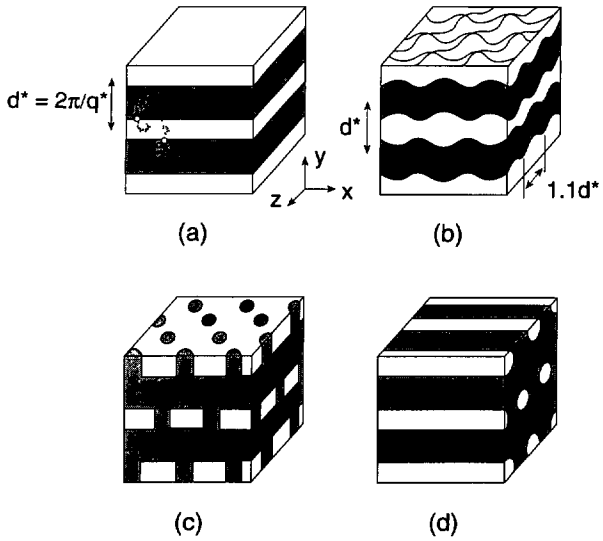

Fig. 1. — Sketches of morphologies of diblock copolymers with $f_1 > 1/2$. (a) Lamellae (LAM), (b) hexagonally modulated lamellae (HML), (c) hexagonally perforated layers (HPL), (d) hexagonally packed cylinders (HEX). These illustrations do not accurately portray the continuous, nearly sinusoidal variation in composition between microdomains near the order-disorder transition.

hexagonally perforated lamellar (HPL) phase forms upon heating from the HML phase.

The molecular origins of this complex phase behavior appears to depend on more than one parameter. We identify compositional asymmetry, f_1, and degree of polymerization, N, as well as an additional conformational asymmetry parameter, ϵ, as the relevant variables. The parameter, ϵ, which we have previously used in a semi-empirical manner [15] is related to the difference in conformational statistics of the two blocks. Here we define more carefully a block asymmetry parameter, which furthermore enters in the form we define it into the theories for conformationally asymmetric block copolymers [4] and homopolymers [16].

There are two parameters that influence how a polymer fills space in three dimensions: molecular volume, V, and conformational volume as characterized by the unperturbed radius of gyration, R_g. There is only one N independent way of combining these factors:

$$\beta^2 = \frac{R_g^2}{V} = \frac{b^2 N/6}{vN} = \frac{b^2}{6v} = \frac{b^2\rho}{6} \tag{1}$$

where v is a segment volume, b is the associated segment length, and $\rho = v^{-1}$ is the segment density. This parameter has been employed previously in theoretical treatments of conformationally asymmetric polymers [4, 16]. The parameter entering directly into the theory is then simply

$$\epsilon = \beta_1^2/\beta_2^2. \tag{2}$$

Here we report a correlation between ϵ and the stacking behavior of the modulated layered phases formed in a variety of model diblock copolymers with $f_1 > \frac{1}{2}$ and $\beta_1 \geq \beta_2$ (i.e. $\epsilon \geq 1$).

Transmission electron microscopy, dynamic mechanical spectroscopy and small-angle neutron scattering experiments have been used to identify phase transitions and phase

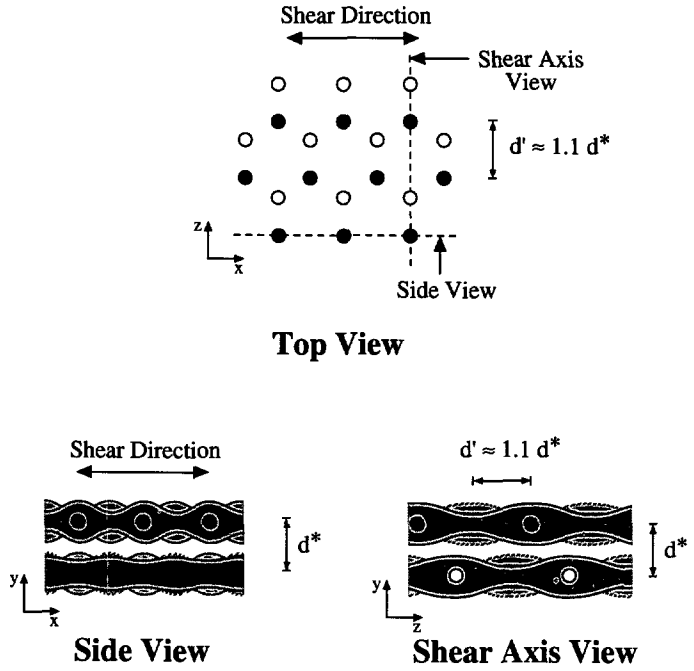

Fig. 2. — ABAB hexagonal stacking behavior of the hexagonally modulated lamellar (HML) microstructure. The coordinates correspond to those given in figure 1 with the HML microstructure in the parallel orientation (see Fig. 11). Solid and open circles denote nodes in the modulated structure for A and B layers. This local stacking arrangement and orientation is observed after the reciprocating shear field has been turned off.

structures in several polyolefin diblock systems. In addition, we discuss briefly an interesting observation of the effect of deuterium substitution on the phase behavior of $f_1 = 0.65$ diblocks and the kinetics of growth from metastable phases. We present data from a series of poly(ethylene) - poly(ethylene-propylene) (PE-PEP), poly(ethylene-propylene)-poly(ethylethylene) (PEP-PEE), poly(ethylene) - poly(ethylethylene) (PE-PEE), and poly(vinylcyclohexane) - poly(ethylethylene) (PVCH-PEE) samples in support of our picture of diblock copolymer phase behavior. The structures of these polymers are shown in figure 3.

The paper is organized as follows. After summarizing experimental procedures in section 2, results are presented in four parts in section 3: transmission electron microscopy, dynamic mechanical measurements, isotope and kinetic effects, and finally small-angle neutron scattering (SANS). We then discuss and summarize our results, and relate them to the phase behavior of other mesomorphic systems in section 4.

2. Experimental.

Full details of the synthesis and characterization of PEP-PEE, PE-PEE and PE-PEP are given elsewhere [17]. Here we merely summarize the general methods. The deuterated polyolefin diblocks were synthesized by catalytic deuteration of poly(diene) precursors, which were anionically polymerized from butadiene and isoprene monomers (obtained from the Aldrich Chemical Company). The precursor for poly(ethylene) is poly(1,4-butadiene), that for poly(ethylethylene)

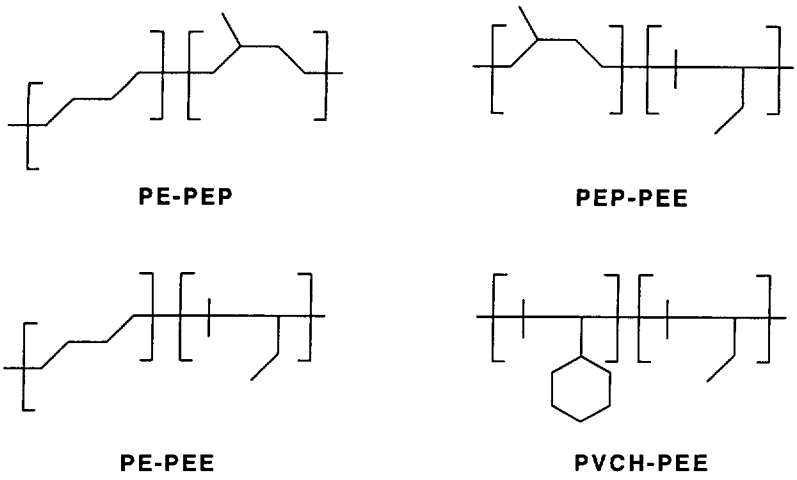

Fig. 3. — Chemical structures of the diblock copolymer systems described in this work.

is poly(1,2-butadiene) while that for poly(ethylene-propylene) is poly(1,4-isoprene). The deuteration did not lead to the stoichiometric addition of two deuterons to each double bond. From experiments on homopolymers of similar molecular weight it was found instead that four or five deuterons are associated with each PEP repeat unit, with only about two attached to a PEE unit. The excess of deuterium on the PEP block is sufficient to provide contrast for the SANS experiments. In some cases deuterated butadiene monomers (from MSD Isotopes) were used in the polymerization, leading to strong contrast between the blocks for neutron scattering experiments. Table I includes an abbreviated nomenclature for the deuteration chemistry. The letter H or D in parentheses indicates the monomer type for each block, while the letter not in parentheses indicates hydrogenation or deuteration of the precursor. For example, the first entry is PEP-PEE-8D with a deuteration notation H(D)-H(D). This indicates that the precursor molecule was fully hydrogenous and was saturated using deuterium.

For the polyolefin containing PVCH, a monodisperse poly(styrene) - poly(1, 2-butadiene) diblock copolymers was anionically synthesized in cyclohexane using a lithium counterion. A two step saturation process was completed using a homogeneous Wilkinson's catalyst, followed by a $Pd/BaSO_4$ heterogeneous catalyst. The resulting poly(vinylcyclohexane) - poly(ethylethylene) (PVCH-PEE) has a deuterium labelled PVCH block providing excellent contrast for SANS experiments. A more detailed report discussing the two step saturation process has been given elsewhere [18]. Although sample PVCH-PEE-1 has $f_1 < \frac{1}{2}$ (see Tab. I), the ϵ value is so close to unity that the phase behavior near the ODT is similar to that for $f_1 > \frac{1}{2}$. Evidence for this trend will also be presented for PE-PEP diblocks, which also have a small ϵ value, in a separate publication [8].

The block microstructures were characterized using ^{1}H-NMR, as described elsewhere [19]. The number average molecular weights and composition were determined from the synthesis stoichiometry, which is a reliable measure of the molecular weight. In addition, light scattering experiments were performed on selected polyolefin diblocks or diene precursors for PE-PEP and PE-PEE copolymers to determine weight-average molecular weights. Molecular weight polydispersities were determined using size exclusion chromatography (SEC) on the polyolefin diblock copolymers and diene diblock precursors. For all polymers the molecular weight dis-

tribution was narrow ($M_w/M_n < 1.1$).

For the transmission electron microscopy experiments, ruthenium tetroxide was used as a staining agent for several polyolefin samples containing poly(ethylene). The rubbery amorphous component is preferentially stained, i.e. the PEP block in PE-PEP diblocks and the PEE block in PE-PEE diblocks. This staining derives from the reduced diffusivity of RuO_4 in the semi-crystalline microdomains, as described in detail elsewhere [20]. Here we simply note that samples were annealed under vacuum at the desired temperature for about one hour before rapid quenching in liquid nitrogen, which ensures trapping of the morphology due to crystallization of the poly(ethylene) blocks (melting temperature ~108 °C). Experience with numerous PE-PEE and PE-PEP specimens has shown that crystallization of the PE block under these conditions does not disrupt the qualitative morphological features. Then ultrathin section (~70 nm) samples were microtomed at −90 °C. Sections were exposed to ruthenium tetroxide vapour for a few hours at room temperature prior to the TEM experiments, carried out on a Jeol 100CX electron microscope operating at 100 kV.

Viscoelastic experiments were performed using a Rheometrics RSA II rheometer operated with a shear sandwich fixture. Phase transitions were located by following the temperature dependence of the dynamic elastic shear modulus, G', and the dynamic loss shear modulus, G'', at frequencies well below that corresponding to the single copolymer chain relaxation time [10]. Small strains were applied, either 2% or 5%, ensuring little deviation from linear viscoelastic behavior. For all samples, we also measured numerous isothermal frequency scans, some of which are presented here.

In one case an RMS-800 dynamical mechanical spectrometer was used for the rheology experiments using a cone and plate geometry (50 mm separation, cone angle $\alpha = 0.04$ rad). The shear moduli measured at low strain amplitudes do not depend on the shear geometry, so that results from different rheometers are quantitatively comparable.

For the small-angle neutron scattering (SANS) studies monodomain samples of the copolymer were studied during and after shear. The shear was applied using a specially constructed oscillatory shear machine described elsewhere [10], which operates with a simple shear geometry. This instrument imposes a reversing (reciprocating) steady shear on the specimen with variable instantaneous shear rates from $0.002 \leq \dot{\gamma}/s^{-1} \leq 4.2$, for a 1 mm gap. Experiments reported here were conducted with 1 mm, 0.33 mm or 0.25 mm thick specimens that were subjected to 100%, 300% or 400% strain amplitudes respectively. The corresponding absolute shear rates are obtained using $| \dot{\gamma} | = 2\gamma\omega/\pi$, where γ is the dimensionless strain and ω is the oscillation frequency. In addition, samples presheared on another oscillatory shear machine were cut-up in three orthogonal planes, so that morphologies could be studied in different sample orientations with respect to the shear direction.

Two classes of SANS experiments are reported here: i) those with the shear field on ($| \dot{\gamma} | > 0$), and ii) after the shear was stopped ($| \dot{\gamma} | = 0$). The application of shear can induce changes in phase behavior such as ordering a disordered melt [21], or restacking a modulated lamellar phase [9] (see below). Because the block copolymers described here lie near the order-disorder transition cessation of shear leads to a relatively facile transition to the true equilibrium state. For most of our experiments the shear field is only used as an alignment tool in order to facilitate phase identification. Although we can never rigorously exclude the possibility of shear-induced metastable states, we have attempted to guard against this circumstance through annealing and complementary rheology and SANS measurements on unsheared specimens that have been quenched from the disordered state.

The SANS experiments were conducted at the 12 meter SANS facility at Risø National Laboratory, Roskilde, Denmark and the NIST/Exxon/University of Minnesota 30 meter instrument at the National Institute of Standards and Technology (NIST), Gaithersburg, Maryland. At

Risø we used $\lambda = 6$ Å neutrons and wavelength distribution $\Delta\lambda/\lambda = 0.09$. At NIST, we used $\lambda = 5.5$ Å neutrons and wavelength distribution $\Delta\lambda/\lambda = 0.14$. Neutron scattering data were collected on an area detector and are reported in arbitrary units of intensity.

3. Results.

3.1 TRANSMISSION ELECTRON MICROSCOPY. — TEM images were obtained for several PE-PEE diblocks and the sample PE-PEP-9D. We present results for the latter, which stained better. Transmission electron micrographs for PE-PEP-9D are shown in figure 4. For the hexagonally modulated lamellar phase the sample preparation procedure follows that for the SANS experiments described in reference [9]. This was done in order to ensure well-aligned lamellae; a confirmation of the structure of this phase requires views in planes both parallel and perpendicular to the layers. The sample was first heated into the isotropic state at 185 °C for 10 min to anneal out defects, then quenched in liquid nitrogen. The sample was subsequently heated to 130 °C for shear orientation under a 100% strain reciprocating shear field at $| \dot{\gamma} | = 0.029$ s^{-1} for 22 h. After stopping the shear, the sample was quenched in liquid nitrogen, microtomed and stained prior to TEM. The shearing was done in a parallel plate device similar to the one used *in situ* for the SANS experiments. A typical TEM image obtained from a sample cut perpendicular to the shear direction is shown in figure 4a. In this projection (modulated) lamellae are clearly visible; note that the actual modulations are not readily seen by TEM due to a relatively small amplitude. In the shear plane, the TEM images are largely featureless (not shown here), consistent with a structure which is modulated rather than perforated. In fact, hexagonal perforations were never seen even after annealing at 130 °C. The hexagonally modulated lamellar structure (see Fig. 1) is consistent with that inferred from the scattering data (see below) and confirms the previous interpretation of SANS data from a $f_{PEP} = 0.65$ PEP-PEE specimen [9].

For the hexagonally perforated layer phase a pre-sheared sample was simply annealed at 143 °C for about one hour prior to liquid nitrogen quenching. A typical TEM picture is shown in figure 4b. Regions of lamellae viewed "side on", with "catenoidal" type perforations arranged hexagonally are clearly visible. This is consistent with the hexagonally perforated layer structure, previously inferred for the high temperature hexagonal mesophase in PEP-PEE-9D from SANS data [9].

Finally, figure 4c shows a TEM image for the high temperature ordered phase of PE-PEP-9D obtained from a sample annealed at 162 °C prior to rapid quenching. This particular section reveals the presence of hexagonally packed cylinders, seen both end-on and sideways, also consistent with the SANS results described below.

3.2 DYNAMIC MECHANICAL MEASUREMENTS. — Rheological experiments can be used to locate order-order phase transitions in block copolymers. At a frequency well below the single chain relaxation time, where dynamic processes occurring on mesoscopic lengthscales are probed, it is often sufficient to follow the temperature dependence of the shear moduli at one fixed frequency. This is illustrated in figure 5 for the system of PE-PEE diblocks. Although we have shear modulus data for all of the samples listed in table I, we focus here solely on the PE-PEE diblocks. These are particularly well suited for viscoelastic measurements due to their low molecular weights. This ensures that the single chain relaxation time corresponds to a high enough frequency so that microstructural viscoelasticity can be studied over a wide frequency window. We note here that PE is semi-crystalline below $\sim$ 108 °C, so that all data presented here is obtained at temperatures higher than this.

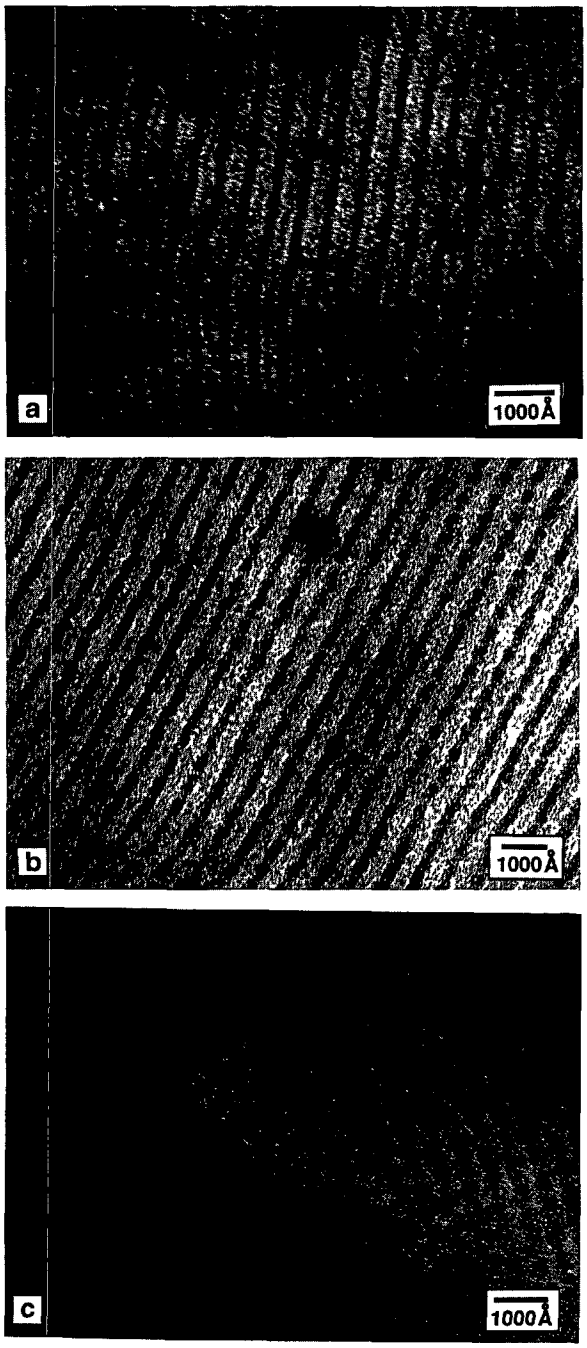

Fig. 4. — TEM pictures for PE-PEP-9D, with the PEP component stained with RuO_4. (a) The sample was sheared and annealed at 120 °C, quenched and cut perpendicular to shear direction. The corresponding image is consistent with a hexagonally modulated lamellar (HML) structure. Note that the amplitude of the modulations is too small to be resolved by TEM. (b) A similar procedure was applied at 143 °C leading to hexagonally perforated layers (HPL). (c) Image of hexagonally packed cylinders obtained from an unsheared sample that was annealed at 162 °C. Both end-on and side views of the cylinders are visible in this projection.

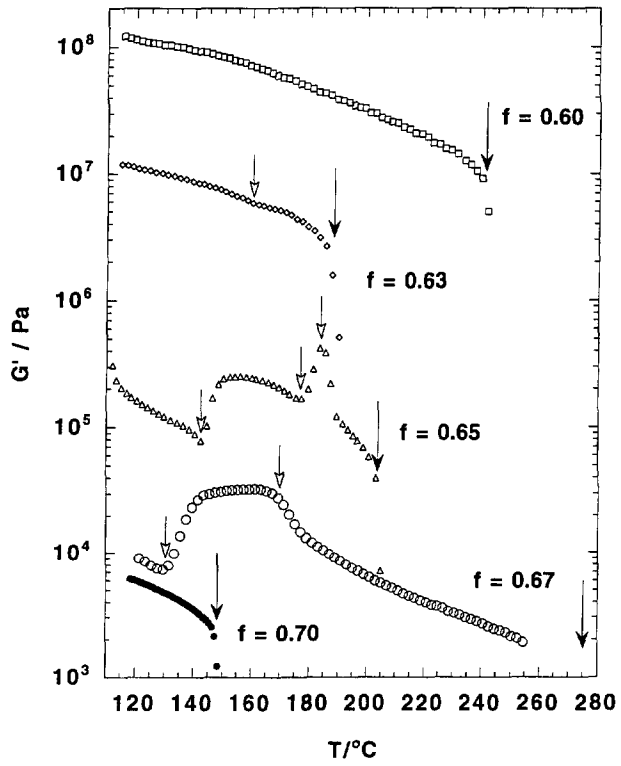

Fig. 5. — Representative heating ramps of the dynamic elastic shear modulus for poly(ethylene) - poly(ethylethylene) (PE-PEE) diblock copolymers obtained at a fixed frequency of 1 rad/s. The solid arrow indicates the ODT, while open arrows show OOT's. (•) PE-PEE-7H (1 °C/min). The curve has been shifted down by a factor 0.1. (○) PE-PEE-12H (1 °C/min). The curve has been shifted up by a factor 10. Successive curves have also been displaced with respect to each other by a factor of 10. (△) PE-PEE-6D (2 °C/min), (◇) PE-PEE-15D (2 °C/min), (□) PE-PEE-17D (2 °C/min).

It is clear from figure 5 that there are no discontinuities in the temperature dependence of the dynamic elastic shear modulus, G', for PE-PEE-17D. This indicates that there are no order-order phase transitions in this sample, a conclusion that is confirmed by studies of the temperature variation of the full frequency response. Although the time-temperature superposition principle cannot be rigorously applied to ordered block copolymers, it has previously been observed that the WLF equation and superposition principle can be applied to the frequency response curves for the lamellar state of block copolymers above a critical reduced frequency ω_c' [22]. We also found that the frequency response data could be superposed for PE-PEE-17D, across the full temperature range of the ordered phase, which has been identified from SANS experiments as lamellae.

For PE-PEE-15D, one order-order transition is observed from an increase in G' and G'' at 160 °C. (Order-order phase transition temperatures (OOT's) are listed in Tab. I.) Although this change is not very pronounced at the frequency used (it is more noticeable in G'', not shown), a change in morphology is confirmed by qualitatively distinct frequency responses on either side of 160 °C. On the basis of the form of the frequency response curve, and more importantly SANS experiments, the low temperature phase has been identified as lamellae.

Table I. — *Diblock copolymers studied.*

Sample b1-b2-no.	f_1	[a]Deuteration	M_n kg mol^{-1}	$\epsilon = (\beta_1/\beta_2)^2$ (at 150°C)	T_{OOT} °C(±2°C)	T_{ODT} °C (±2°C)	[b]Ordered phases
PEP-PEE-8D	0.65	H(D)-H(D)	76	1.7	70	92	H(M/P)L-HEX
PEP-PEE-9D	0.65	"	94	"	87, 137, 147	178	LAM-HML-HPL-HEX
PEP-PEE-9H	0.65	H(H)-H(H)	94	"	95, 145, 178	19	LAM-HML-HPL-HEX
PEP-PEE-16D	0.68	H(D)-H(D)	93	"	92	160	HML-HEX
PEP-PEE-20D	0.70	"	98	"	None	212	HEX
PE-PEP-11D	0.60	H(D)-H(D)	150	1.5	166, 172	177	HML-HPL-HEX
PE-PEP-9D	0.65	"	150	"	137, 147	172	HML-HPL-HEX
PE-PEE-17D	0.60	H(D)-H(D)	42	2.5	None	212	LAM
PE-PEE-15D	0.63	'	43	"	160	187	LAM - H(M/P)L
PE-PEE-5D	0.65	"	36	"	127	164	H(M/P)L - HEX
PE-PEE-6D	0.65	"	43	"	138, 175, 180	202	LAM-HML-HPL-HEX
PE-PEE-6H	0.65	H(H)-H(H)	43	"	143, 177, 184	204	LAM-HML-HPL-HEX
PE-PEE-12H	0.67	H(H)-D(H)	40	"	133, 175	275	LAM-HPL-HEX
PE-PEE-7H	0.75	"	44	"	None	148	HEX
PVCH-PEE-1	0.35	H(D)-H(H)	65	0.95	185	210	HML-MCYL

(a) H(D) refers to a hydrogenous polydiene precursor block that was deuterated. b. HML - hexagonally modulated lamellae; HPL - hexagonally perforated layers; HEX - hexagonally packed cylinders; LAM lamellae; MCYL - modulated hexagonally packed cylinders.

Comparison of frequency sweeps for other samples suggests that the high temperature phase may be hexagonally modulated lamellae or hexagonally perforated layers. The temperature ramps in figure 5 indicate that PE-PEE-12H possesses three ordered phases, which have distinct frequency responses (not shown). The $f_1 = 0.75$ sample PE-PEE-7H has no OOT's, and on the basis of SANS the single ordered phase in this sample has been identified as hexagonally packed cylinders [23].

The $f_1 = 0.65$ samples, PE-PEE-6D and PE-PEE-6H each appear to exhibit four ordered phases, based on isochronal measurements of G' as a function of temperature, shown in figure 5 for PE-PEE-6H. This isochronal behavior of G' (and also G'', not shown) as a function of temperature is remarkably similar to that of the $f_1 = 0.65$ PEP-PEE-9D sample which was the subject of a previous publication [9]. However, the phase behavior of PE-PEE-6D appears to be subtly distinct from that of PE-PEE-6H, as revealed by detailed studies of the viscoelasticity of these systems. We return to a discussion of this in the next section. Figure 6 shows typical frequency sweeps for the distinct phases in the PE-PEE diblocks, using PE-PEE-6H as an example because it has four ordered phases. Based on similarities in the viscoelastic properties of this system and PEP-PEE-9D shown elsewhere [9], and the identification of the phases in the latter using SANS, the phases in PE-PEE-6H can be inferred. The low temperature phase is lamellae. Heating produces hexagonally modulated lamellae (HML), followed by a hexagonally perforated layer (HPL) phase and then hexagonally packed cylinders at the highest temperatures, prior to disordering.

Before proceeding to a discussion of isotope and kinetic effects, we observe that the dynamic loss modulus for all PE-PEE samples in lamellar and hexagonally packed cylinder phases can be superposed to a fair approximation. This superposition does not apply for the intermediate

states, with typical frequency responses shown in figure 6. Also, G' data for different morphologies cannot be superposed. The similarity of G'' data in lamellar and hexagonally packed cylinder phases may be due to the fact that the structure in both cases can be considered to be built of layers, without three-dimensional connectivity. Three-dimensional order leads to a solid-like G' response which is much less frequency dependent (see Fig. 6). Such behavior is seen for bicontinuous phases or body-centered cubic sphere phases [12, 24]. The response of a perforated phase and a sphere phase might be expected to be similar, since these can be considered to be simply inverted with respect to each other.

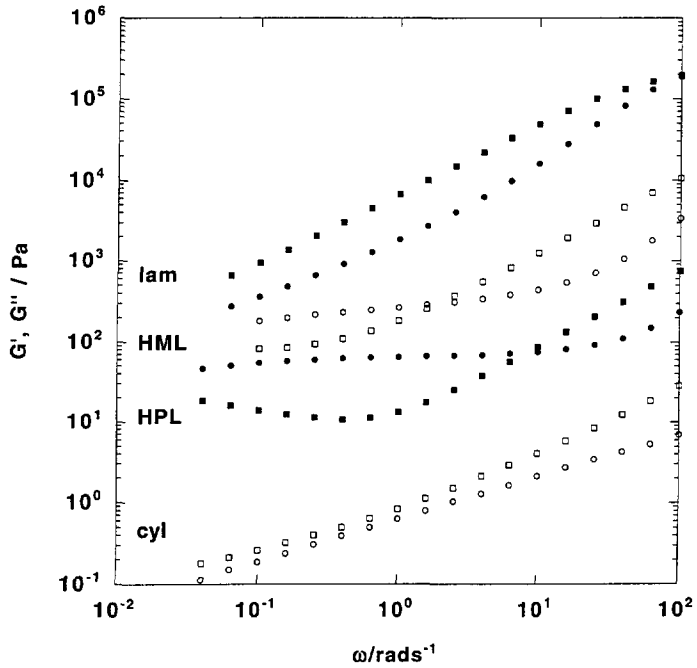

Fig. 6. — Representative frequency sweeps for PE-PEE-6H, showing the four ordered phases: lamellae at 115 °C, hexagonally modulated lamellae at 151 °C, hexagonally perforated layers at 160 °C, hexagonally packed cylinders at 197 °C. The curve for HML has been shifted down by a factor of 10, that for HPL by a factor of 100 and that for cylinders by a factor 1000.

The temperature dependence of the dynamic shear moduli for PVCH-PEE-1 is shown in figure 7 for a quenched sample (i.e. one cooled from the disordered state without shear) and for a shear-oriented sample. In both cases, one order-order phase transition at 185 °C is evident, while the order-disorder transition is $\simeq$ 210 °C (there are no sharp discontinuities in the viscoelastic response at the ODT for the shear-oriented sample). Characteristic frequency sweeps for these sample conditions at 195 °C are shown in figure 8. The frequency response of the sheared sample is consistent with a shear-oriented cylinder phase (compare this frequency sweep with that for cylinders in Fig. 5), while that for the quenched sample resembles what we usually observe for unoriented cylinders [21]. In the latter case, it is to be expected that the low frequency behavior is more solid-like than for the former, as incompletely aligned cylinders shear less easily than oriented cylinders along their axis of alignment.

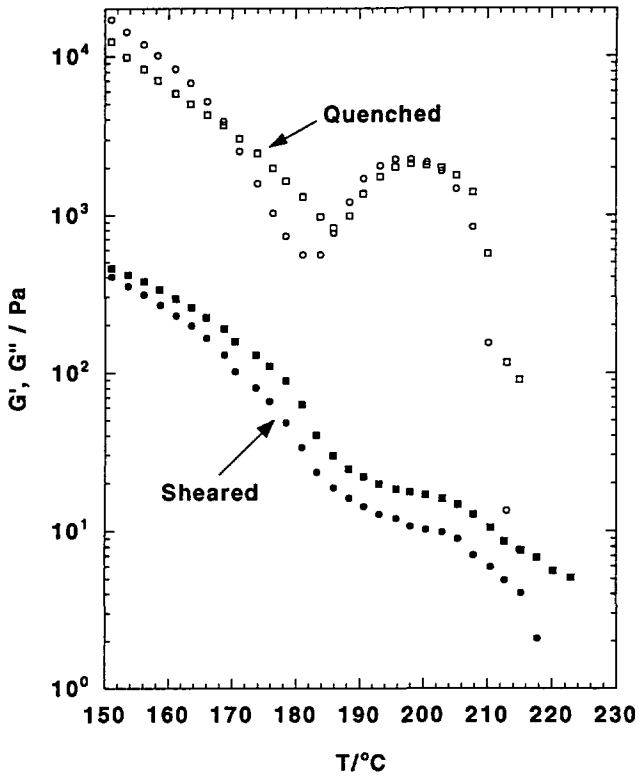

Fig. 7. — Heating ramps of the dynamic elastic shear moduli for PVCH-PEE-1. The heating rate was 0.5 °C/min and the frequency 0.2 rad/s; circles: G', squares: G''. The quenched data (open symbols) were obtained without prior shearing, while the sheared data (filled symbols) were taken after shearing at 150 °C at 0.1 rad/s with 100% strain amplitude.

The dynamic mechanical spectroscopy data presented above (which is a representative selection from a large amount of data on these systems) enables the boundaries for complex phase behavior between lamellar and hexagonally packed cylinder phases in diblocks with $f_1 > \frac{1}{2}$ to be located as approximately $f_1 = 0.63$ and $f_1 = 0.70$. For identification of the structures, we turn to SANS experiments, discussed in section 3.4.

3.3 ISOTOPE AND KINETIC EFFECTS. — An unexpected variation in the phase behavior of $f_1 = 0.65$ diblocks has been observed depending on their deuterium content. For PEP-PEE-9 we have samples prepared by deuteration (PEP-PEE-9D) and hydrogenation (PEP-PEE-9H) of the hydrogenous poly(diene) precursor. The deuterated specimens have been described in previous publications [9], and these results suggested a certain sensitivity to isotopic substitution [26]. PEP-PEE-9H also has four ordered phases, and based on comparison of the frequency responses in the four ordered phases, they appear to be the same as those identified for PEP-PEE-9D in reference [9]. However, there is a significant difference in the order-disorder transition for these polymers: PEP-PEE-9D disorders at 178 °C, while PEP-PEE-9H disorders at 195 °C (these values are the temperatures at which the dynamic elastic moduli start to decrease towards zero).

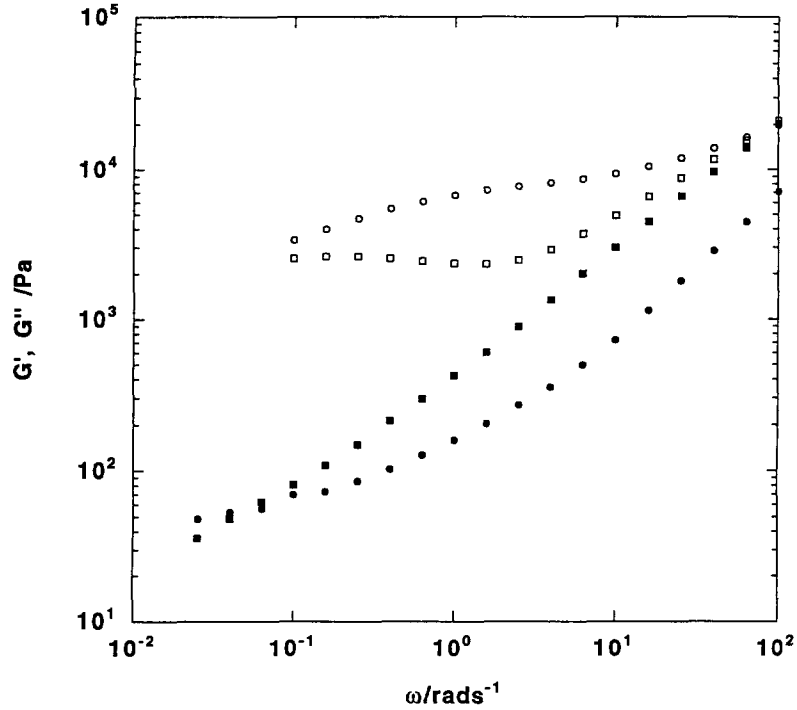

Fig. 8. — Frequency sweeps for PVCH-PEE-1 at 195 °C; circles: G', squares: G''. The open symbols correspond to a specimen quenched from the disordered state, and the filled symbols from a specimen sheared as indicated in figure 7.

Here we present data for two PE-PEE-6 samples, one of which exhibits phase behavior very similar to that of the PEP-PEE-9 diblocks. Frequency sweeps taken in the second ordered phase of PE-PEE-6H at 151 °C, separated by a 50-min time interval, are shown in figure 9. The elastic moduli stabilize within one hour with a response very different from that for the third ordered phase also shown in figure 9. In the latter case, the data were measured at 160 °C and the elastic moduli only stabilize after $2\frac{1}{2}$h. By comparing this frequency-dependent elastic modulus data with that for PEP-PEE-9D, these two phases were identified as hexagonally modulated lamellae and hexagonally perforated layers. It is important to note that these detailed studies of the dynamics of the growth of complex phases indicate that the second order-order phase transition "at equilibrium" is between 151 °C and 160 °C. Temperature ramps, such as that for PE-PEE-6H shown in figure 5 (and reproduced in the inset of Fig. 9), should be used with caution in locating the precise temperature of order-order phase transitions. This is especially true for "topological" transitions, such as HML to HPL, since these appear to be most kinetically restricted.

This comment is graphically supported by data for PE-PEE-6D, where the viscoelastic frequency response was followed as a function of time at 150°C, then 165 °C, and finally 183.5 °C. At the higher temperature, the dynamic elastic moduli stabilized rapidly to give the frequency response curves shown in figure 10, in which G' is high and weakly dependent on frequency. This type of frequency response characterizes "connected" structures such as the hexagonally perforated layer phase or bicontinuous morphologies. Comparison with PE-PEE-6H and PEP-PEE-9D enables us to identify this phase as hexagonally perforated layers.

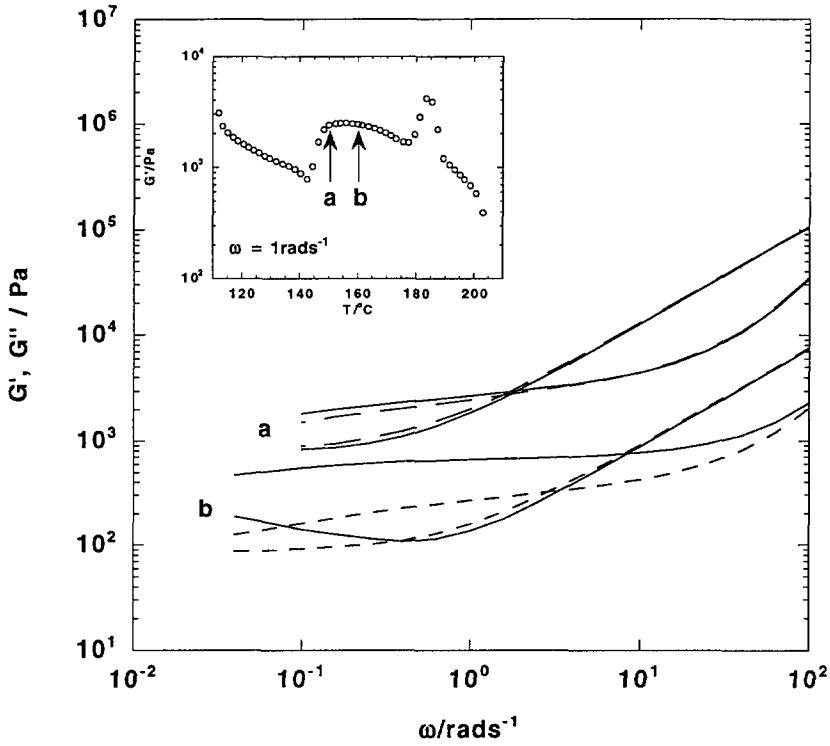

Fig. 9. — Frequency sweeps for PE-PEE-6H obtained in the intermediate hexagonal phase region as a function of annealing time. The inset shows the temperature dependence of G' at 0.1 rad/s for a heating rate of 2 °C/min. Dashed lines denote the first of a series of frequency sweeps, solid lines the last; (a) at 151 °C, time between sweeps = 50 min; (b) at 160 °C, time between sweeps = 2.5 h. The curves in (a) have been shifted vertically one decade.

At 165 °C, the dynamic elastic moduli stabilize in a curve which is superposable upon that at 183.5 °C, although this curve takes longer to evolve (~4 h). At 150 °C we observed that initially the frequency response curves resemble those for the hexagonally modulated lamellar phase in PE-PEE-6H (Fig. 9) or PEP-PEE-9D. However, the frequency response curves begin to evolve slowly towards the form stabilized at higher temperatures. We estimate that at this temperature it would take 1-2 days for the hexagonally perforated layer phase to grow in, but that this is the "equilibrium" phase. Therefore, PE-PEE-6D has three equilibrium ordered phases, whereas PE-PEE-6H has four, which are also those observed for the PEP-PEE-9 samples. For the latter, the hexagonally modulated lamellar phase appears to be an equilibrium phase, whereas for PE-PEE-6D it is a metastable state accessed as the hexagonally perforated layer phase grows in. The growth is more rapid as the temperature within this phase is increased. We believe these results indicate that the equilibrium phase boundary between hexagonally modulated lamellae and hexagonally perforated layers for these systems lies close to $f_1 = 0.65$, and subtle changes in deuterium content of the diblocks are sufficient to alter the free energy balance for these phases.

3.4 SMALL-ANGLE NEUTRON SCATTERING. — We have SANS data for many of the samples listed in table I. Here, we present a (necessarily small) representative selection of this data. In

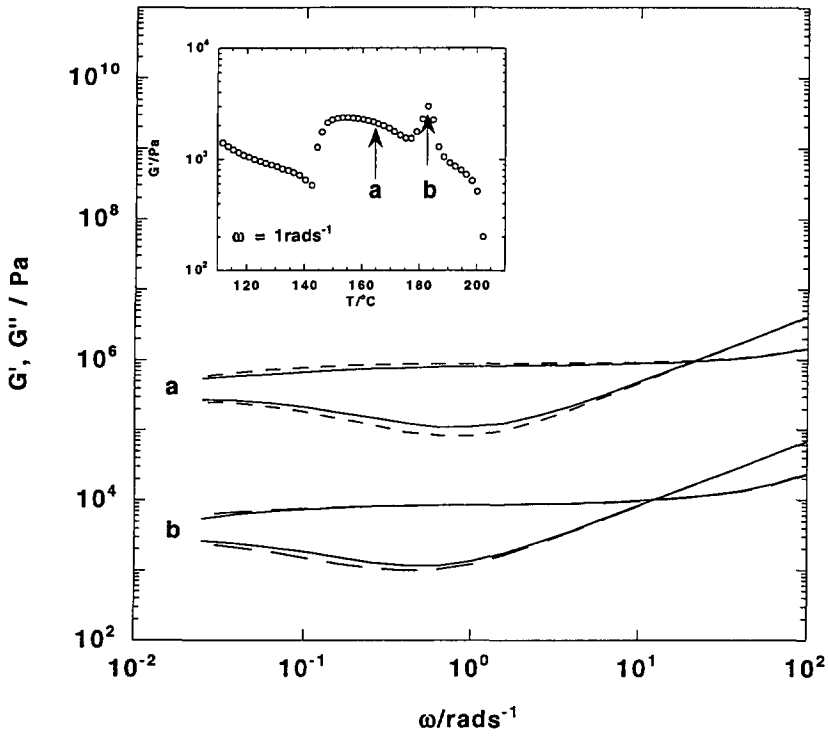

Fig. 10. — Frequency sweeps for PE-PEE-6D obtained in the intermediate hexagonal phase region as a function of annealing time. The inset shows the temperature dependence of G' at 0.1 rad/s for a heating rate of 2 °C/min. Dashed lines denote the first of a series of frequency sweeps, solid lines the last; (a) at 165 °C, time between sweeps = 4 h, (b) at 183.5 °C, time between sweeps = 3 h. The curves in (a) have been shifted vertically one decade.

particular, the universal existence of hexagonally modified lamellar phases formed on heating from the lamellar phase is demonstrated. PVCH-PEE-1 is considered first since the HML structure proposed by us is most clearly established for this system. Because PVCH has a glass transition temperature at $T_g \cong 140$ °C, the HML phase could be frozen, and characterized at room temperature by directing the neutron beam along the x, y and z axes (see Fig. 1) using cut specimens. This procedure is not convenient with any of the other materials. When dealing with layered diblock copolymer microstructures near the ODT, two different domain orientations can be produced by application of dynamic shearing [9, 10]. These are referred to as parallel and perpendicular orientations, as illustrated in figure 11. In general, high shear rates provide access to the perpendicular form while low shear rates result in a parallel geometry. In conducting this research we have exploited this effect in order to obtain neutron beam access along two microstructure directions while the specimen was mounted in the *in situ* shearing device.

Representative results for PE-PEE-12H obtained with both orientations in the shear cell are presented next. These will illustrate features common to all the hexagonally layered phases. In particular, the behavior under shear in the parallel orientation, previously discussed for PEP-PEE-9D, is again observed. However, for PE-PEE-12H and PEP-PEE-9D there are differences in the SANS patterns obtained on perpendicularly oriented samples. In particular,

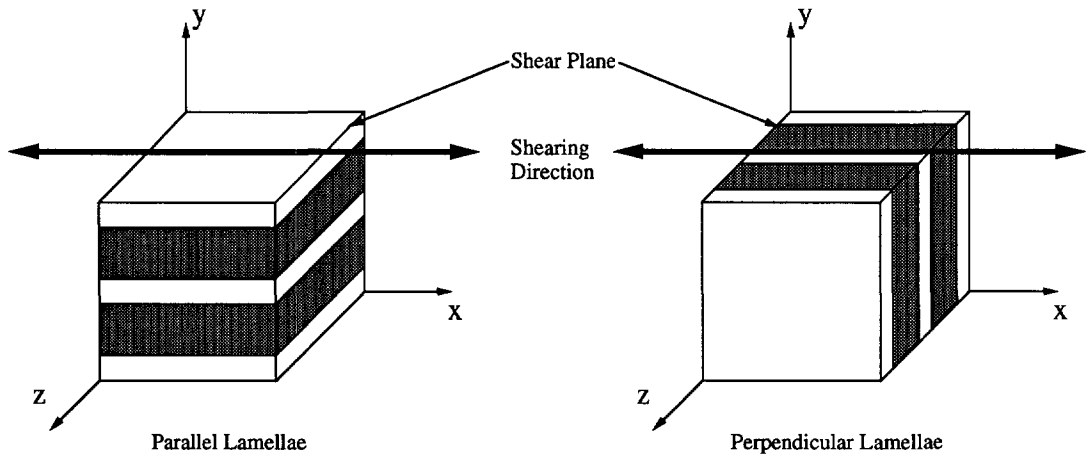

Fig. 11. — Two layered microstructure orientations can be obtained through dynamic shearing (10). The parallel orientation generally occurs when low shear rates are applied, while the perpendicular one is generated by high shear rates. This effect provides neutron beam access (y - direction) to two different microstructure orientations while shearing.

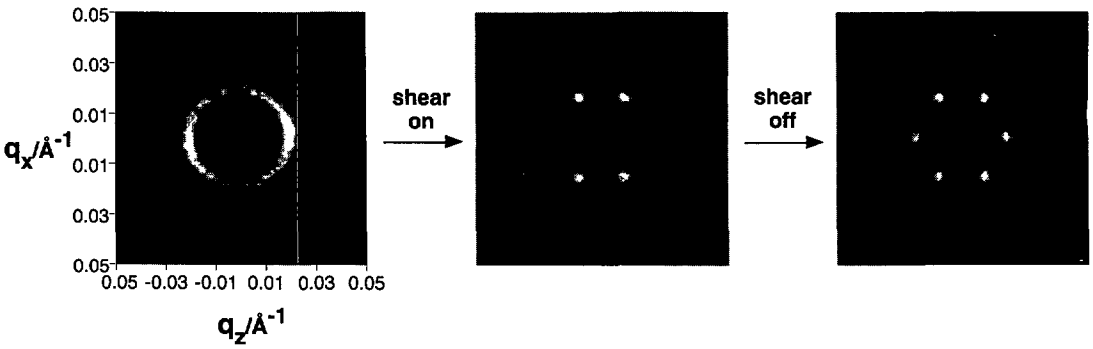

Fig. 12. — SANS patterns for PVCH-PEE-1 in the parallel orientation (see Fig. 11) of the hexagonally modulated lamellar (HML) phase. The data are shown with 16 gray levels on a linear scale. Left: at 170 °C without shear, center: at 168 °C under shear with $|\dot{\gamma}| = 0.64\ s^{-1}$, right: without shear at 168 °C.

the off-equatorial side peaks are located such that the wavevectors do not form a closed loop, in contrast to PVCH-PEE-1. It is as yet unclear whether this observation is connected to a coupling between shear and sample orientation in these samples, although all data illustrating phase behavior were obtained after switching off the reciprocating shear field used to align specimens; we also illustrate some behavior under shear for these diblocks.

First, SANS patterns for PVCH-PEE-1 are presented. Behavior under shear in the low temperature hexagonally modulated lamellar phase in the parallel orientation is illustrated by figure 12. At 170 °C in the absence of shear, a (weakly anisotropic) ring of scattering is observed. After large amplitude shearing (400% at $|\dot{\gamma}| = 2.6\ s^{-1}$), the four spot pattern (with a weak underlying isotropic ring) is obtained. After switching off the shear field, this pattern

evolves into the hexagonal pattern of equal intensity peaks shown at the right of this figure. The loss of the two equatorial reflections under shear was also observed for PEP-PEE-9D, and was discussed in an earlier work [9]. It is consistent with a restacking transition to a monoclinic-I structure under shear.

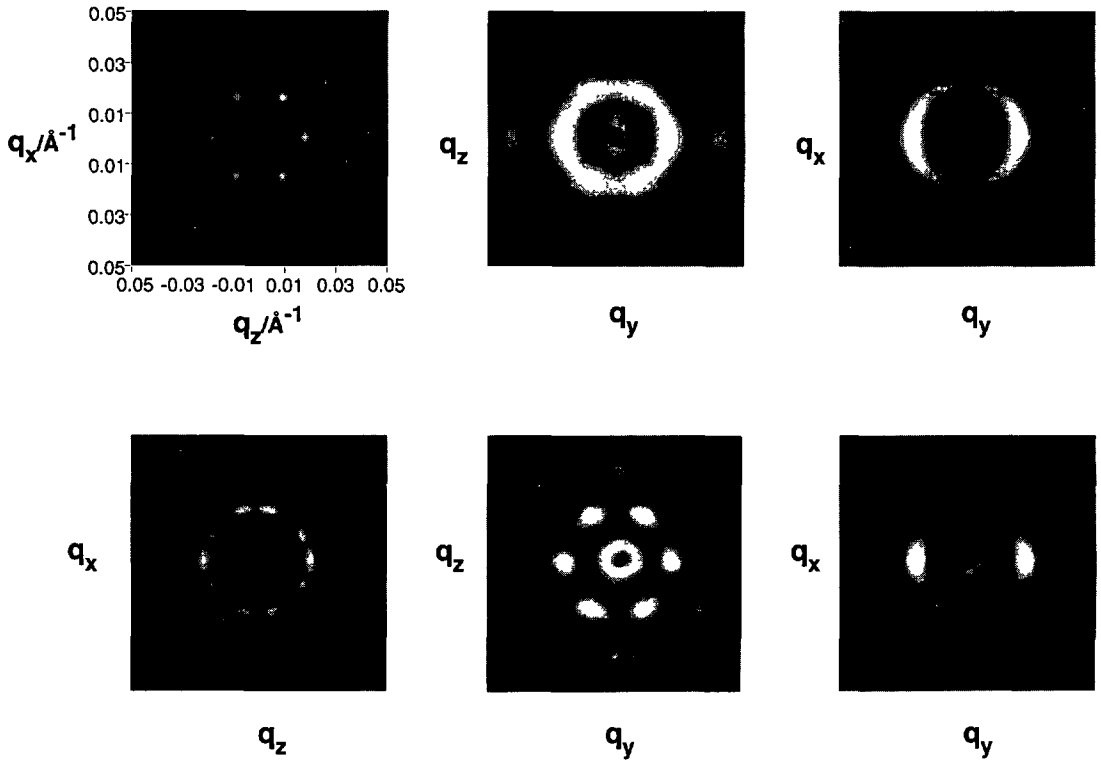

Fig. 13. — SANS patterns for PVCH-PEE-1 in three orthogonal planes in the HML (top panels) and MCYL (lower panels) phases. For the $q_y - q_z$ and $q_x - q_y$ planes the data (shown on a logarithmic scale) were obtained from samples sheared *in situ*, cooled below T_g for PVCH, cut along different planes, and placed in the neutron beam. The data for the $q_x - q_z$ plane (corresponding to the parallel orientation in Fig. 11) were obtained from samples mounted in the shear cell (data shown on a linear scale). Top: $q_x - q_z$ plane at 168 °C, $q_y - q_z$ plane cooled from 180 °C, $q_x - q_y$ plane cooled from 180 °C. Bottom: $q_x - q_z$ plane at 195 °C, $q_y - q_z$ plane cooled slowly from 195 °C, $q_x - q_y$ plane cooled from 195 °C.

Small-angle neutron scattering patterns for both the ordered phases in PVCH-PEE-1 are shown in figure 13 for three orthogonal orientations of the sample. The data for the $q_x - q_z$ plane (parallel orientation in Fig. 11) were obtained for samples in the shear cell (in the absence of shear), while the data for the other planes was obtained for samples cooled from the ordered phase below the glass transition temperature of PVCH [27]. We found that this procedure preserves the qualitative features of the SANS pattern, and hence the underlying morphology. The data for the low temperature phase are consistent with a hexagonally modulated lamellar phase. In the $q_y - q_z$ and $q_x - q_y$ planes, equatorial reflections are observed at q^* and $2q^*$, where

$q^* \simeq 1.1q'$, with q' the shortest wavevector (i.e., that observed for the hexagonal pattern in the $q_x - q_z$ plane), consistent with a layered structure. The first order side peaks close to 60°, which are most pronounced in $q_y - q_z$, result from the modulated structure, as do the higher order off-equatorial peaks at $1.7q^*$ and $2q^*$. The unit cell symmetry is thus close to hexagonal. Absence of the (001) reflection in $q_y - q_z$, which should appear for hexagonal (ABAB) stacking of the modulations, can be rationalized on the basis of imperfect alignment along q_z; note that the most effective alignment is obtained along the shear direction (x) and gradient (y).

For the high temperature phase, ten reflections are observed at q^* in the $q_x - q_z$ plane. We will return to a discussion of this phase shortly. The pattern in the $q_y - q_z$ plane indicates a hexagonally packed cylinder structure (with the (10) plane parallel to $x - z$, also confirmed by sample rotation experiments), consistent with the preceeding interpretation of the rheology data. However the weak side peaks at $\theta = 56 \pm 3°$ in $q_x - q_y$ indicate that this phase cannot simply be parallel hexagonally packed cylinders. Instead this data, together with the weak ten spot scattering pattern in the $x - y$ plane, suggest that the cylinders are modified as described in the following section.

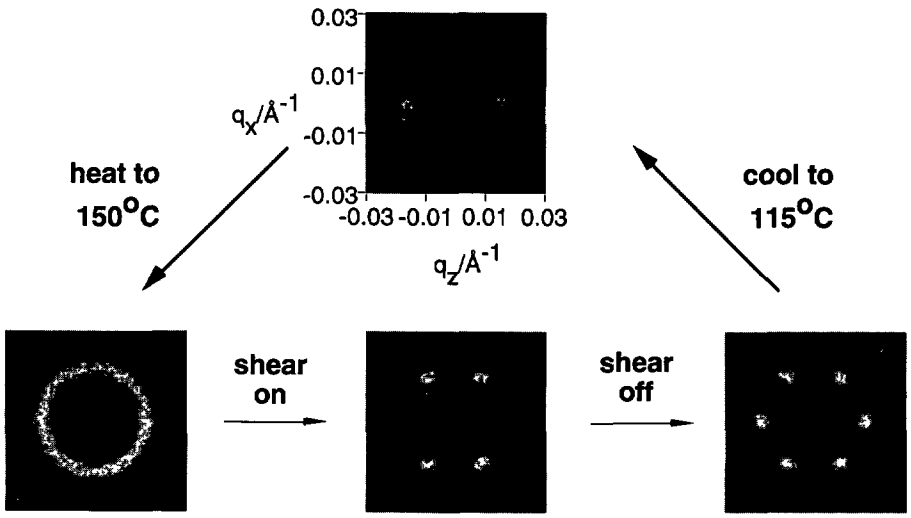

Fig. 14. — Effect of variation of shearing conditions and temperature on SANS patterns in the parallel orientation (see Fig. 11) for PE-PEE-12H. The data are shown on a linear scale. This behavior is analogous to that reported earlier for PEP-PEE-9D (9).

The neutron scattering data shown in figures 14 and 15 for PE-PEE-12H provide strong evidence for transitions from lamellae to hexagonally perforated layers to hexagonally packed cylinders (see Fig. 1) on heating. Detailed studies of the influence of shear and temperature on the structure in the parallel orientation are summarized in figure 14. This behavior resembles that previously reported for PEP-PEE-9D, and that for PVCH-PEE-1 shown in figure 12, which illustrates the universality of the in-plane hexagonal order in the modulated and perforated layer phases. The data for PE-PEE-12H in the perpendicular orientation in figure 15 suggest that the layer stacking in the phase formed from lamellae on heating differs from that previously reported for PEP-PEE-9D.

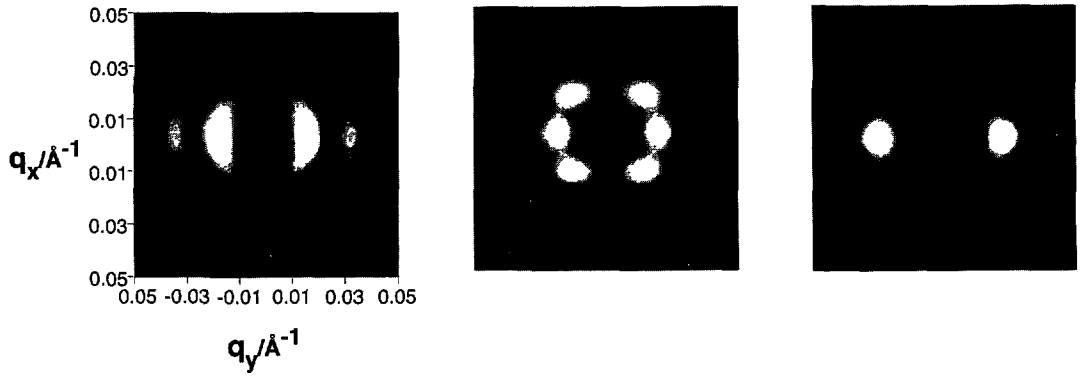

Fig. 15. — SANS patterns for PE-PEE-12H in the perpendicular orientation (see Fig. 11). The data are presented on a logarithmic scale to show highr order reflections. Left: 115 °C, center: 150 °C, right: 200 °C

The SANS pattern shown in figure 14 (top), with a slightly anisotropic ring of weak scattering is consistent with a low temperature (parallel) lamellar phase. Upon reheating to 150 °C without shear, a pronounced ring of scattering appears (the count rate at the detector was observed to increase by a factor of about 8) which transforms on shearing at $\mid \dot{\gamma} \mid = 0.64\ s^{-1}$ to the hexagonal pattern of unequal intensity peaks shown in the center. As discussed for PEP-PEE-9D [9], an unequal distribution of peak intensities is consistent with a restacking transition under shear. The hexagonal ordering is suppressed along the shear direction, but transforms into a hexagonal pattern of equally intense spots immediately after cessation of shearing (center right).

The difference in the ordering of the hexagonal mesophase in PE-PEE-12H compared to either of the hexagonal mesophases in PEP-PEE-9D is illustrated most graphically by the SANS patterns in the perpendicular orientation (Fig. 15), obtained by the application of high frequency, 100% strain shearing. The equatorial peaks with commensurate harmonics at $2q^*$, $3q^*$ and $4q^*$ observed for the low temperature mesophase are consistent with lamellae. On heating, side peaks at $(45 \pm 1°)$ develop without shearing of the sample. This is in contrast to the behavior of PEP-PEE-9D, where shear is required to observe the incommensurate side peaks, which in that sample are near 50° in both mesophases. In addition, for PE-PEE-12H (which has large neutron scattering length density contrast between the blocks) higher order reflections are observed in this phase. Four peaks are observed at $q = (1.75 \pm 0.05)q^*$, $\theta = 24 \pm 2°$ with respect to the equator. In addition, the higher order equatorial reflections are at $q = (1.75 \pm 0.05)\ q^*$, rather than $2q^*$ as observed for the HML phase of PEP-PEE-9D. We are unable to index the reflections of this pattern to a monodomain crystal structure. It appears to be either a system with incommensurate lengthscales forming a hexatic phase, or a crystal structure twinned about many different crystal planes. In either case there is no macroscopic translational order. The intensity of the side peaks relative to the principal equatorial reflections (see Fig. 16) suggest a hexagonally perforated layer phase, rather than a hexagonally modulated lamellar phase, an identification supported by TEM images.

For this sample, the position of the first order peaks jumps on crossing the first order-order transition, while the second order ones stay in the same location. Large amplitude shearing at low frequencies results in sharp spots in the hexagonally perforated layer phase (Fig. 15, center). This is in contrast to the mechanical behavior of the hexagonally perforated layer

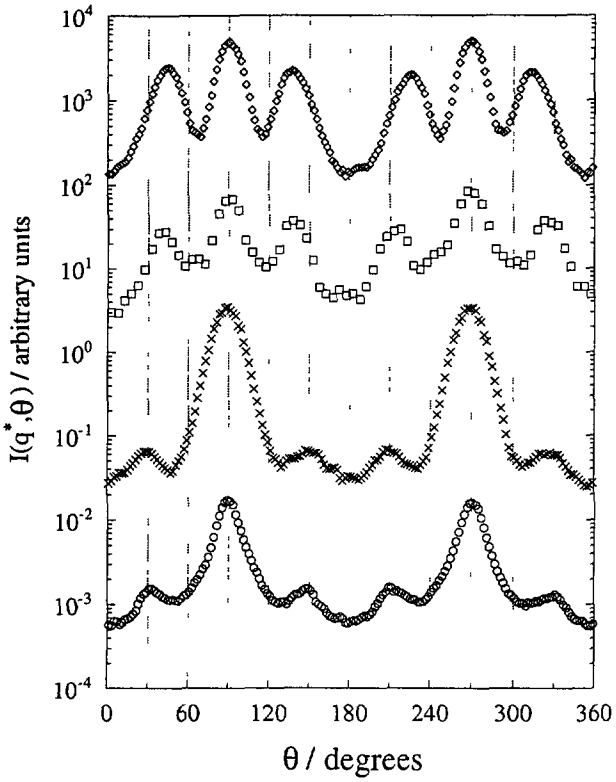

Fig. 16. — Angular scans of SANS data at the principal wavevector q^* for intermediate phases of diblocks in the perpendicular orientation (see Figs. 1, 2 and 11). $\theta = 0$ (or 180 °) is defined by the x axis, which is coincident with the shear direction. From top to bottom: PE-PEE-12H at 150 °C (q band: 0.017-0.023 $Å^{-1}$), PEP-PEE-9D at 146 °C (q band: 0.014-0.017 $Å^{-1}$), PE-PEP-9D at 115 °C (q band: 0.0055 - 0.0095 $Å^{-1}$) PVCH-PEE-1 at 180 °C (q band: 0.017-0.023 $Å^{-1}$). Data sets have been rescaled to give similar intensity ranges and shifted vertically. In PVCH-PEE-1 and PE-PEP-9D the off-equitorial peaks occur at nearly ± 60° while for PEP-PEE-9D and PE-PEE-12H this angle is 52° and 45°, respectively.

phase in PEP-PEE-9D which cannot support shear and instead transforms into cylinders. On further heating above the order-order transition at 175 °C the SANS pattern transforms into the two arcs shown on the right hand side of figure 15. Again, in contrast to PEP-PEE-9D, this transformation occurs without the application of a large amplitude shear field.

The scattering pattern in the hexagonal mesophase for PE-PEE-12H in the perpendicular orientation is thus subtly different from that for PEP-PEE-9D, although it has the same symmetry elements. More importantly, it appears that the hexagonal in-plane structure can develop in an ordered manner, without requiring application of a large amplitude shear field. Furthermore, this phase can withstand shearing and the transformation to hexagonally packed cylinders is only observed on heating.

Figure 16 presents the essential features of the SANS data for the perpendicular orientation of hexagonally layered phases in two systems where the wavevectors are matched in two dimensions, and two where they are not. The angular dependence of the scattered intensity in a band centered on q^* is shown, where q^* is the wavevector associated with the layer pe-

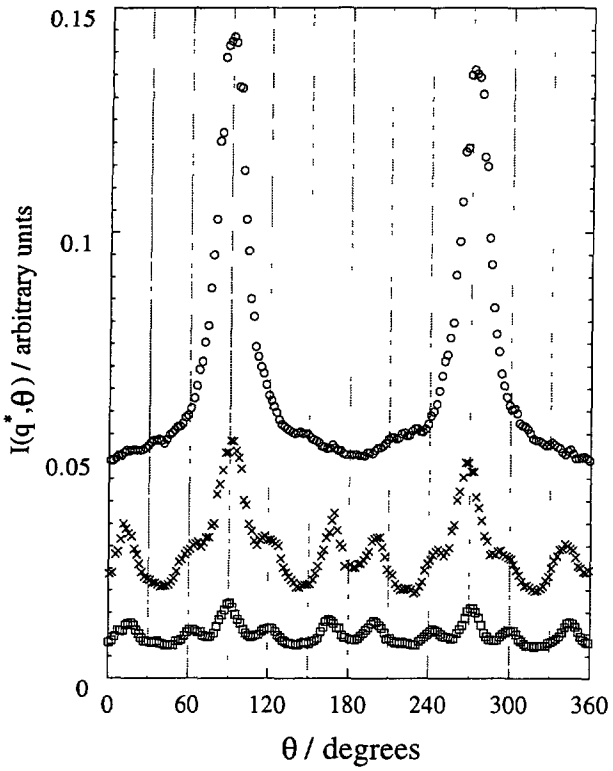

Fig. 17. — Angular scans of SANS data for PVCH-PEE-1 in a "perpendicular" orientation as a function of temperature. The q band was centered on q^* ($0.017 < q < 0.023$ Å^{-1}). The measured counts at the detector were divided by the monitor counts to give the $I(\theta)$ values shown. Circles: 185 °C (shearing at $|\dot{\gamma}| = 2.6$ s^{-1}), crosses: heated to 195 °C (without shear), squares: cooled from 195 °C to 170 °C.

riodicity, d^* (i.e. $q^* = 2\pi/d^*$). A previous publication was devoted to a study of the phase behavior of PEP-PEE-9D, and two-dimensional SANS patterns are presented in reference [9]. The hexagonally modulated lamellar phase has additional higher order equatorial layering peaks at $2q^*$. High order side peaks are not observed. No higher reflections are observed for the hexagonally perforated layer phase, for which an angular scan through the peaks at $1.1q^* = q' = 0.0160 \pm 0.0002$ Å^{-1} is shown in figure 16. Side peaks occur at 52±2°, whereas in the lower temperature hexagonally modulated lamellar phase they are at 48±2°. In both cases, the wavevectors corresponding to the side peaks and equatorial peaks are unmatched in two dimensions.

For PEP-PEE-9D the side peaks for the hexagonally perforated layer phase (see Fig. 16) are about 6-8 times more intense than those associated with the HML phase, when normalized by the principal equitorial peaks [9]. Instead of the structure with no long-range translational order implied by incommensurate wavevectors, a structure with three dimensional periodicity could be obtained by hypothesizing the existence of higher order reflections at $q = 1.69q'$, $\theta = 65°$ to the principal peaks, which are however not observed [9].

The side peaks at $q^* = 0.0182 \pm 0.0002$ Å^{-1} for the second ordered phase (see Fig. 15) of PE-PEE-12H at 150 °C are at $45 \pm 2°$ with respect to the principal equatorial reflections.

We note in passing that viscoelastic experiments reveal a "shoulder" near 140 °C, which may be a transient hexagonally modulated lamellar phase, from which the hexagonally perforated layer phase grows. Since the side peaks are rather intense (50% peak intensity) compared to the layering peaks, by analogy with PEP-PEE-9D, this phase is identified as hexagonally perforated layers. Here we note that the distinction between modulations and perforations may become ambiguous for specimens that exhibit only one intermediate hexagonal phase, such as PE-PEE-12H.

For the PVCH-PEE diblock, the angular scans centered on q^* show that the first order side peaks are at, or very close to, the wavevector matching condition $\theta = 60°$. (Based on fitting of this data using Lorentzians on top of a linear sloping background under each side peak, the average angle of the side peaks with respect to the equatorial ones is found to be 58.5°). For this sample higher order reflections at or close to angles 30° and 90° to the equator are also observed at $1.7q^*$ (together with additional peaks at $2q^*$, including equatorial reflections). The low intensities of the side peaks relative to the equatorial reflections indicates that both systems form hexagonally modulated lamellar phases.

The remarkable scattering pattern in figure 13 (lower left panel) with ten spots close to q^* evolves from a two spot pattern, characteristic of a hexagonally packed cylinder phase, as shown by the angular scans through the SANS data presented in figure 17. This suggests epitaxial growth of the new structure from a two-dimensional hexagonal template. On cooling back to the lower temperature phase, the ten spots remain, but with a significant reduction in intensity, as shown by data at 150 °C in figure 17. Thus the high temperature phase supercools, but with a reduction in order. Evidence for this modified hexagonally packed cylinder phase is also present in the $q_x - q_y$ scattering plane (Fig. 13) as off-equitorial reflections at q^*, similar to those obtained from the modified layered structures.

4. Discussion.

In summary, we have shown that the transition near the order-disorder transition from lamellae to hexagonally packed cylinder phases in diblock copolymers with $f_1 = 0.63$-0.70 proceeds *via* intermediate layered phases with hexagonal in-plane order. In addition, we have found two routes to complex phase behavior in these asymmetric diblocks. In the first, a hexagonally perforated layer phase is formed when lamellae become unstable with the modulation wavevector incommensurate with the layering wavevector and unmatched in two dimensions [9]. In the second, matched wavevectors in the hexagonally modulated lamellar phase enable a transition to a three-dimensional modified cylinder phase at higher temperatures. The diblock copolymer phase diagram for the systems considered here is not symmetric about $f_1 = \frac{1}{2}$ (with the likely exception of PVCH-PEE-1). For $f_1 < \frac{1}{2}$, the region of complex phase behavior is confined to roughly $f_1 = 0.34$-0.43, and phases distinct from those for $f_1 > \frac{1}{2}$ (e.g. cubic bicontinuous) are observed [11-14].

There is no universal phase diagram for the systems we have discussed. Rather, the specific phase behavior of a diblock depends on a combination of molecular parameters, of which f and χN were included in the classical mean field picture [3]. The parameter $\bar{N} = b^6 N/v^2$, where N is the degree of polymerization, was introduced when composition fluctuations were considered [28-30]. Since the experimental phase diagrams are asymmetric about $f_1 = \frac{1}{2}$, it is necessary to specify a third parameter associated with conformational asymmetry. We speculate that there may be a connection between the degree of the incommensurability of wavevectors in the

perpendicular orientation and the differences in chain packing reflected by the conformational asymmetry parameter ϵ. Thus, the "most incommensurate" system we have studied, PE-PEE-12H, where the first-order side peaks are furthest from the wavevector matching condition, and additionally the higher order reflections are incommensurate with the first order ones, has the largest ϵ value, $\epsilon_{PE-PEE} \cong 2.5$ at 150 °C. In contrast, PVCH-PEE-1 where ϵ is closest to unity, $\epsilon_{PVCH-PEE} \cong 1.05$ at 150 °C, has a HML phase with matched wavevectors, and PEP-PEE-9D is intermediate between these limits, where $\epsilon_{PEP-PEE} \cong 1.7$ at 150 °C. If we hypothesize that conformational asymmetry leads to two competing lengthscales in the system, then the formation of incommensurate and modulated lamellar phases could be rationalized by models similar to that proposed for thermotropic smectics by Prost and coworkers [31]. (Here we note that there is no clear molecular origin for a second length scale. One possibility is conformational or compositional asymmetry driven in-plane modulations that could be traced to asymmetric non-Gaussian chain stretching.) In these models, the competition between two lengthscales corresponding to the molecular length and to the dipolar association leads to a large number of possible smectic A and smectic C polymorphs. However, a phase with in-plane hexagonal order has yet to be considered. Smectic liquid crystals can relieve the frustration from the two lengthscales by forming tilted phases, a degree of freedom presumably unavailable to flexible copolymer coils, which instead form an in-plane modulated structure.

An unusual isotope dependence of phase behavior at $f_1 = 0.65$ was noted. Although it has been established that phase transition temperatures for polymers are dependent on the degree of deuteration [32, 33], an influence of deuterium content on the kinetics of formation of metastable phases is unanticipated. We believe that it reflects the subtle balance between free energies of hexagonally modulated lamellar and hexagonally perforated layer phases at $f_1 = 0.65$.

The composition fluctuations in the lamellar phase which lead to the phase transition to a hexagonally layered phase are necessarily anisotropic, a factor that has recently been incorporated in fluctuation theories. Smectic liquid crystal modes of deformation of lamellae have recently been included in Fredrickson and Binder's [30] parameterization of Brazovskii [28] fluctuation theory [34, 35]. The elastic modes of deformation of lamellar phases are compression and splay, where the latter means that the angle between layer normals varies through the sample. However, consideration of these modes alone gives a modulated lamellar state which is never stable with respect to the undeformed lamellar phase [33]. It appears that a successful theory for modulated lamellar phases must account for two lengthscales, as in the Prost model [36].

The parameter $\bar{N}$ is a Ginzburg parameter for the composition fluctuations, i.e. it controls their magnitude. For the lamellar phase of symmetric diblocks, Fredrickson and Helfand [29] showed that the shift in the order-disorder transition temperature varies as $\bar{N}^{1/3}$. It has yet to be established how order-order transitions depend on $\bar{N}$ in fluctuation theory, which has yet to be applied to complex phases. Brazovskii *et al.* [37] extended Brazovskii's original fluctuation theory [28] to consider structures that can be stabilized when wavevector dependence of the fourth order vertex functions is included (this changes the relative weights of cubic and fourth order terms in a Landau free energy expansion). They found that two phases with BCC symmetry and an FCC phase could become stable in three dimensions, in addition to one-dimensional (lamellar) and two-dimensional hexagonal phases; square and hexagonal phases in two dimensions may also be stable. They also considered two types of orthorhombic structures, and found that both were not stable. Thus it remains an open question to account for our observations theoretically, although anisotropy of fluctuations should play an important role (and was not considered by Brazovskii *et al.*).

The remarkable SANS pattern shown in figure 13 for the high temperature ordered phase of PVCH-PEE-1 may represent a manifestation of such anisotropic fluctuations. This dense distribution of reflections at q^* could be interpreted as a precursor, in the ordered state near the ODT, of the fluctuations on a sphere at q^* in the disordered state, which Brazovskii showed drives a weakly first order phase transition to the ordered state.

In separate publications [8, 11-14] we demonstrate that a bicontinuous cubic phase, with Ia$\bar{3}$d space group symmetry, occurs in a variety of diblock copolymers near the ODT. This phase appears to always be bounded by hexagonal cylinders, the HPL phase, and disorder at high temperatures. We also find that as $\bar{N} \to \infty$ the Ia$\bar{3}$d structure disappears, while it is stabilized by decreasing molecular weight [8]. The combination of $\bar{N}$, χN, and f for PVCH-PEE-1 places it in close proximity to the conditions where we expect this bicontinuous phase to first emerge. This raises the fascinating possibility that the high temperature phase constitutes a fluctuation driven modulated cylinder phase, where the modulations (perhaps undulations) assume a packing symmetry that anticipates the impending Ia$\bar{3}$d state. In fact, the 10-spot pattern found in the $q_x - q_z$ scattering plane (Fig. 13) is strikingly similar to that documented for the Ia$\bar{3}$d phase when epitaxially grown from an oriented hexagonal cylinder morphology [12]. Therefore, we cannot rule out the possibility that the high temperature structure reflects a two-phase state, with the scattering patterns representing the sum of oriented hexagonally packed cylinders and the epitaxially grown Ia$\bar{3}$d microstructure. However, the results do not really support this model. The $q_z - q_y$ scattering show no evidence of second-order $(2\bar{2}0)$ cubic reflections, that have been documented in pure epitaxially grown material [12], and the angular dependence of the first-order reflections in $q_x - q_z$ are slightly different from those required by the Ia$\bar{3}$d symmetry. Moreover, the weak off-equitorial reflections in $q_x - q_y$ are not consistent with our previous epitaxial growth model [12].

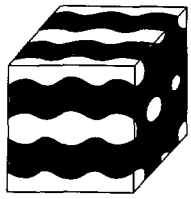

Fig. 18. — Illustration of a modulated hexagonally packed cylinder (MCYL) microstructure. This sketch is not intended to reflect a particular modulation (undulation) packing symmetry.

Therefore, we believe a modulated hexagonally cylinder (MCYL) phase exists between the HML and disordered states in PVCH-PEE-1. A schematic illustration, that depicts an undulating microstructure is presented in figure 18; this cartoon is not necessarily drawn with the proper overall modulation packing symmetry. Clearly, the fluctuations that stabilize such a structure will be coupled to the highly anisotropic hexagonal cylinder packing, leading to a non-cubic modulation packing symmetry. Although we cannot assign an unambiguous space group to this morphology at the present time, we suspect it will exhibit symmetry elements similar to the Ia$\bar{3}$d state, which it appears to anticipate.

We conclude with several remarks of a more general nature. The hexatic phase was first observed in thermotropic liquid crystals [36]. The layering instability for diblocks with $f_1 > \frac{1}{2}$ where the wavevectors are incommensurate and unmatched in 2D may lead to the formation of

a hexatic phase. Our observations on modulated and incommensurate layered phases suggests that diblock copolymer phase behavior (especially in the region f_1=0.63-0.70) is analogous to some of the rich mesomorphism of thermotropic liquid crystals. Of course, since phase transitions are observed in diblocks that are one component systems on varying the temperature, we can be certain of formal thermotropism. However, complex mono- or bi-continuous phases observed in diblock copolymers (which will be discussed in greater detail elsewhere [11, 13]) are similar to those in lyotropic liquid crystals (as are those occurring at low f_1 in diblocks). However, the interfacial properties of diblocks near the ODT are quite different from those of lyotropics. The composition profile for diblocks is essentially sinusoidal (as can be deduced from the absence of observed higher order reflections for the complex phase SANS data presented here) and the interfacial contribution to the free energy is small. We will show elsewhere that this has important consequences for the symmetry of complex three-dimensional phases [8]. In contrast, lyotropic liquid crystal phases have well-defined interfaces (and scattering patterns contain many higher orders of reflections) and the interfacial free energy is a vital component in determining their overall free energy [1, 39]. This is more akin to the behavior of strongly segregated diblocks. It is clear that the fascinating interrelations between the mesomorphism of these systems will be the subject of much future work.

Acknowledgements.

This work was supported by the Air Force Office of Scientific Research (AFOSR-90-0207 and AF/F49620-93-1-0182). We acknowledge the support of NIST, U.S. Dept. of Commerce and the Center for Interfacial Engineering (CIE) in providing some of the facilities used in this work, and NATO for a travel grant to FSB and KA.

References

[1] Seddon J.M., *Biochim. Biophys. Acta* **1031** (1990) 1.

[2] I. Goodman Ed., Developments in Block Copolymers. 1 (Applied Science, New York, 1982); Developments in Block Copolymers. 2 (Applied Science, New York, 1985).

[3] Leibler L., *Macromolecules* **13** (1980) 1602.

[4] Helfand E., Wasserman Z.R., Developments in Block Copolymers. 1, I. Goodman Ed. (Applied Science, New York, 1982);
Vavasour J.D. and Whitmore M.D., *Macromolecules* **26** (1993) 7070.

[5] Semenov A.N., *Sov. Phys. JETP* **61** (1985) 733.

[6] Thomas E.L., Alward D.B., Kinning D.J., Martin D.C., Handlin D.L., Fetters L.J., *Macromolecules* **19** (1986) 2197.

[7] Hasegawa H., Tanaka H., Yamasaki K., Hashimoto T., *Macromolecules* **20** (1987) 1651.

[8] Bates F.S., Schulz M.F., Khandpur A.K., Förster S., Rosedale J.H., Almdal K., Mortensen K., *Faraday Discuss. Chem. Soc.* to appear.

[9] Hamley I.W., Koppi K.A., Rosedale J.H., Bates F.S., Almdal K., Mortensen K., *Macromolecules* **26** (1993) 5959;
Almdal K., Koppi K.A., Bates F.S., Mortensen K., *ibid* **25** (1992) 1743.

[10] Koppi K.A., Tirrell M., Bates F.S., Almdal K., Colby R.H., *J. Phys. II France* **2** (1992) 1941.

[11] Förster S., Khandpur A.K., Zhao J., Bates F.S., Hamley I.W., Ryan A.T., Bras W., *Macromolecules* to appear.

[12] Schulz M.F., Bates F.S., Almdal K., Mortensen K., *Phys. Rev. Lett.* **73** (1994) 86.

[13] Schulz M.F., Khandpur A.K., Bates F.S., Hajduk D.A., Gruner S.M., in preparation.
[14] Bates F.S., Schulz M.F., Khandpur A.K., Majumdar B., Hajduk D.A., Gruner S.M., Almdal K., Mortensen K., in preparation.
[15] Bates F.S., Schulz M.F., Rosedale J.H., Almdal K., *Macromolecules* **25** (1992) 5547.
[16] Bates F.S., Fredrickson G.H., *Macromolecules* **27** (1994) 1065.
[17] Rosedale J.H., Bates F.S., Almdal K., Mortensen K., Wignall G.D., *Macromolecules* to appear.
[18] Gehlsen M.D., Bates F.S., *Macromolecules* **27** (1994) 3611.
[19] Bates F.S., Rosedale J.H., Bair H.E., Russell T.P., *Macromolecules* **22** (1989) 2557.
[20] Khandpur A.K., Macosko C.W, Bates F.S., *J. Polym. Sci., Polym. Phys. Ed.* to appear.
[21] Koppi K.A., Tirrell M., Bates F.S., *Phys. Rev. Lett.* **70** (1993) 1449.
[22] Rosedale J.H., Bates F.S., *Macromolecules* **23** (1990) 2329.
[23] The $f = 0.75$ PE-PEE specimen was investigated by SANS following procedures reported in reference [21]. Shear oriented material exhibited a hexagonal scattering pattern when the neutron beam was directed along the shear axis and a pair of reflections when directed normal to the shear direction.
[24] Koppi K.A, Tirrell M., Bates F.S., Almdal K., Mortensen K., *J. Rheology* **38** (1994) 999.
[25] Almdal K., Bates F.S., Mortensen K., *J. Chem. Phys.* **96** (1992) 9122.
[26] Previous reports of three ordered phases in PEP-PEE-9D [9] were based on experiments using two samples with different deuterium contents. The heating rate dependence of the elastic moduli was different for the earlier experiments. In addition, the sample orientation on the rheometer may have differed from that for the later report. Thus, it is not clear at present if these differences reflect an isotope effect alone. These issues are presently being investigated in more detail for this and other samples.
[27] Gehlsen M.D., Bates F.S., *Macromolecules* **26** (1993) 4122.
[28] Brazovskii S.A., *Sov. Phys. JETP* **41** (1975) 85.
[29] Fredrickson G.H., Helfand E., *J. Chem. Phys.* **87** (1987) 697.
[30] Fredrickson G.H., Binder K., *J. Chem. Phys.* **91** (1989) 7265.
[31] Prost J., *Adv. Phys.* **33** (1984) 1.
[32] Gehlsen M.D., Rosedale J.H., Bates F.S., Wignall G.D., Hansen L., Almdal K., *Phys. Rev. Lett.* **68** (1992) 2452.
[33] Bates F.S., Wignall G.D., Koehler W.C., *Phys. Rev. Lett.* **55** (1985) 2425.
[34] Amundson K., Helfand E., *Macromolecules* **26** (1993) 1324.
[35] Morse D.C., Milner S.T., *Phys. Rev. E* **47** (1993) 1119.
[36] Hamley I.W., unpublished work.
[37] Brazovskii S.A., Dzyaloshinskii I.E., Muratov A.R., *Sov. Phys. JETP* **66** (1988) 625.
[38] Pershan P.S., Structure of Liquid Crystal Phases (World Scientific, Singapore, 1988).
[39] Tanford C., The Hydrophobic Effect, 2nd ed. (Wiley, New York, 1980).